INTERNATIONAL JOURNAL FOR NUMERICAL METHODS IN FLUIDS
*Int. J. Numer. Meth. Fluids* 2008; **56**:91–114
Published online 23 August 2007 in Wiley InterScience (www.interscience.wiley.com). DOI: 10.1002/fld.1572

# The steady Navier–Stokes/energy system with temperature-dependent viscosity—Part 2: The discrete problem and numerical experiments

Carlos E. Pérez[1,*,†], Jean-Marie Thomas[2], Serge Blancher[3] and René Creff[3]

[1]*Departamento de Ingeniería Matemática, Universidad de Concepción, Casilla 160-C, Concepción, Chile*
[2]*Laboratoire de Mathématiques Appliquées, Université de Pau, BP 1155, 64013 Pau, France*
[3]*Laboratoire de Transferts Thermiques, Université de Pau, France, Hélioparc, Av. Pres. Angot, 64000 Pau, France*

SUMMARY

In this second part, we analyse the associated discrete problem arising from a conforming finite element method formulation of the mathematical model presented in the first part. Thus, existence and uniqueness of the discrete solution when using small enough data are stated following the same strategy used in the continuous case, with a Cea's type error estimate established as the main result. Some numerical experiments, steady and unsteady, are performed, which allow us to validate the previous mathematical model and its discrete approximation. Copyright © 2007 John Wiley & Sons, Ltd.

Received 24 October 2006; Revised 11 June 2007; Accepted 13 June 2007

KEY WORDS: Navier–Stokes; variable viscosity; finite element methods; heat transfer; error estimation; convection

## 1. INTRODUCTION

As long as the thermophysical properties of a fluid are not considered to be constant in the model, or mixed boundary conditions (BCs) are stated for the physical model, Navier–Stokes equations become non-trivial for analysis. This is principally due to the fact that generalizations of many ideas and techniques stated for the homogeneous BCs and constant-property situations are not straightforward.

*Correspondence to: Carlos E. Pérez, Departamento de Ingeniería Matemática, Universidad de Concepción, Casilla 160-C, Concepción, Chile.
†E-mail: carlos@ing-mat.udec.cl

Contract/grant sponsor: Dirección de Investigación of the Universidad de Concepción; contract/grant number: DIUC 204.013.022-1.0

Nevertheless, there are many physical situations in which these kinds of models or sets of BCs are necessary. A good example is an open channel flow, where a fluid particle that leaves the physical domain does not re-enter that domain anymore. For this kind of situation, in order to be able to solve the mathematical problem, it is common to state the outflow or 'do nothing' BCs (following the terminology of Gresho and Sani [1] or Turek and Co-workers [2]), in which some *ad hoc* BCs at the exit region of the channel are chosen, in the hope that their utilization does not influence the main flow characteristics which are to be found.

Despite the existence of numerous articles in fluid dynamics which consider some variations of the thermophysical properties—usually by means of the Boussinesq model—be it theoretically (see [3–7]) or numerically ([8–11] and the references cited therein), and numerous articles in which different kinds or sets of BCs are analysed (see [2, 12–16] and the references therein), to the authors' knowledge, there are only a few works which consider these two difficulties put together, as for instance [17, 18].

In the first part of our paper (cf. [19] hereafter referred as 'Part I'), we have proposed and analysed a model for the study of steady, two-dimensional incompressible Navier–Stokes equations with temperature-dependent viscosity and buoyancy, which is well adapted to open flow problems. We have shown that under sufficiently small and regular prescribed data at the boundary, the mathematical problem is well posed, with a unique result for small data.

The next step in the mathematical analysis is the study of a numerical procedure which allow us to find an approximate solution of the continuous problem. This work will be undertaken here by means of a conforming finite element (FE) discretization. This is not a trivial task, even under a conforming approach, because of the coupling with the energy equation and also because of the imposed outflow BCs, as we shall see in the following sections.

Our main result in this part is the statement of an error estimate for the discrete solutions of a weak formulation of the original problem by considering conforming 'inf–sup' compatible subspaces. Thus, the quality of the numerical approximation becomes related to the quality of the subspace approximation for each variable.

Finally, the last section is devoted to the numerical experiments. Because the dynamics of this kind of coupling are expected to be unsteady, we present steady and unsteady experiments, where the core of the computer code developed is based on the structure of a steady problem (see Remark 1).

We show that even if the main effect is associated with density in the buoyancy term, in some circumstances, the temperature influence on the dynamic viscosity has a non-negligible effect on the main flow characteristics.

## 2. THE CONTINUOUS PROBLEM

Let $\Omega$ be a two-dimensional domain occupied by an incompressible Newtonian fluid. Even if the mathematical analysis presented in the next section is only valid for the two-dimensional case, the model remains valid in the more realistic three-dimensional situation.

We refer here to the steady dimensionless model presented and analysed in Part I. It is based on some physical considerations, which allow us to consider the Boussinesq assumptions. This model is generalized by considering temperature dependence on the thermophysical properties of dynamic viscosity and thermal conductivity.



DOI: 10.1002/fld

By choosing some reference physical quantities, such as length, velocity, time and temperature $T_m$ (more details are given in Part I), we can define the non-dimensional parameters of the flow: the Reynolds number $Re_m$, the Grashof number $Gr_m$, the Péclet and Prandtl numbers $Pe_m$ and $Pr_m$, respectively. Also, we can define the non-dimensional version of the thermophysical properties of dynamic viscosity $\mu^*(T)$ and thermal conductivity $\kappa^*(T)$ as follows:

$$\mu^*(T) = \frac{\mu(T)}{\mu(T_m)}, \quad \kappa^*(T) = \frac{\kappa(T)}{\kappa(T_m)} \tag{1}$$

The main properties considered for these non-dimensional physical properties in the first analysis were their positiveness, uniform boundedness and Lipschitz-continuity.

The reference parameters chosen give the following dimensionless set of equations (asterisks and subscript $m$ were omitted for the sake of simplicity):

$$\mathbf{u} \cdot \nabla \mathbf{u} - \frac{1}{Re} \nabla \cdot (\mu(T) D(\mathbf{u})) + \nabla p = \frac{Gr}{Re^2} T \mathbf{k} + \mathbf{F} \tag{2}$$

$$\nabla \cdot \mathbf{u} = 0 \tag{3}$$

$$\frac{\partial T}{\partial t} + \mathbf{u} \cdot \nabla T - \frac{1}{Pe} \nabla \cdot (\kappa(T) \nabla T) = 0 \tag{4}$$

In (2), $\mathbf{k}$ is the unitary vector acting in the direction opposite to gravity. We provide Equations (2)–(4) with the following BCs: prescribed values for velocity and temperature at the entry and the walls, and prescribed *zero traction forces* and *zero flux density* at the exit. These BCs are obtained as follows:

$$\begin{cases} \mathbf{u} = \mathbf{u}_e(\mathbf{x}) & \text{at the inflow} \\ \mathbf{u} = \mathbf{0} & \text{at the walls} \\ \boldsymbol{\sigma}(\mathbf{u}, p) \cdot \mathbf{n} = \mathbf{0} & \text{at the outflow} \end{cases}, \quad \begin{cases} T = T_e(\mathbf{x}) & \text{at the inflow} \\ T = T_u(\mathbf{x}), T_l(\mathbf{x}) & \text{at the walls} \\ (\kappa(T) \nabla T) \cdot \mathbf{n} = 0 & \text{at the outflow} \end{cases} \tag{5}$$

In (5), $\boldsymbol{\sigma}(\mathbf{u}, p)$ is the stress tensor, which depends on the temperature due to the viscosity variation: $\boldsymbol{\sigma}(\mathbf{u}, p) = -p\boldsymbol{\delta}_{ij} + 1/Re_m \mu(T) D(\mathbf{u})$, where $D(\mathbf{u})$ is the deformation tensor (the symmetric part of $\nabla \mathbf{u}$) and $\boldsymbol{\delta}$ is the Kronecker tensor.

For the mathematical analysis, we consider $\Omega$ to be an open, two-dimensional, bounded and convex domain with a Lipschitz boundary $\partial\Omega$. We assume that we have a set $\Gamma_D \subseteq \partial\Omega$ of positive measure, and we set $\Gamma_N = \partial\Omega \backslash \Gamma_D$. The portion $\Gamma_D$ is the part of the boundary associated with the Dirichlet BCs for velocity and temperature, and $\Gamma_N$ is associated with the outflow BCs as stated in (5). These hypotheses concerning the geometry will be considered hereafter.

We restate the BCs of (5) as follows:

$$\mathbf{u} = \mathbf{u}_D, \quad T = T_D \text{ on } \Gamma_D \tag{6}$$

$$\boldsymbol{\sigma}(\mathbf{u}, p) : \mathbf{n} = 0, \quad (\kappa(T) \nabla T) \cdot \mathbf{n} = 0 \text{ on } \Gamma_N \tag{7}$$

In (6), the surface function $T_D$ takes the prescribed values of temperature at the entry and at the walls, which are supposed to be uniformly bounded, that is, there exist two real constants $T_1$ and $T_2$, such that

$$T_1 \leqslant T_D(\mathbf{x}) \leqslant T_2 \quad \text{on } \Gamma_D \tag{8}$$



DOI: 10.1002/fld

In (8), due to the non-dimensional temperature definition $T^* = (T - T_m)/\Delta T$, the value of $T_1$ is not necessarily positive. We have shown in the first part that if no internal energy generation is allowed in the model, the temperature remains bounded by these uniform constants in the whole domain.

The set of BCs (6)–(7) suggest naturally the use of the following well-known functional vector spaces: let $L^2(\Omega)$ be the standard Lebesgue space, with norm $\|\cdot\|_0$. We set:

$$H^1(\Omega) = \left\{ v \in L^2(\Omega),\ \frac{\partial v}{\partial x_i} \in L^2(\Omega) \text{ for } i = 1, 2 \right\} \tag{9}$$

$$H^1_{0,\Gamma_D}(\Omega) = \{ v \in H^1(\Omega),\ v|_{\Gamma_D} = 0 \} \tag{10}$$

$$H^{1/2}(\Gamma_D) = \{ \eta \in L^2(\Gamma_D),\ \exists v \in H^1(\Omega),\ v|_{\Gamma_D} = \eta \} \tag{11}$$

where $v|_{\Gamma_D}$ is the partial trace of a function $v \in H^1(\Omega)$. The analogous vector-valued spaces will be denoted by bold symbols, for instance: $\mathbf{H}^1_{0,\Gamma_D} = H^1_{0,\Gamma_D} \times H^1_{0,\Gamma_D}$. The norm associated with a Hilbert space $H^m(\Omega)$ will be denoted by $\|\cdot\|_m$. The scalar product associated with the $L^2(\Omega)$ norm will be denoted as $(\cdot,\cdot)_{0,\Omega}$ or just $(\cdot,\cdot)$ if it is unambiguous. Throughout this paper, $C$, with or without subscript, denotes a generic positive constant depending only on $\Omega$ and $\Gamma_D$. The value of $C$ may differ at different occurrences.

Following [20], for the elements in $H^1_{0,\Gamma_D}$, we have Poincaré's and Korn's inequalities as follows:

$$\|v\|_0 \leqslant C \|\nabla v\|_0 \quad \forall v \in H^1_{0,\Gamma_D} \tag{12}$$

$$\|\mathbf{v}\|_1^2 \leqslant C(\|\mathbf{v}\|_0^2 + \|D(\mathbf{v})\|_0^2) \quad \forall \mathbf{v} \in \mathbf{H}^1_{0,\Gamma_D} \tag{13}$$

The weak form of (2)–(4) with BCs (6)–(7) is the following: let $\mathbf{u}_D$ be given in $\mathbf{H}^{1/2}(\Gamma_D)$ and $T_D$ given in $H^{1/2}(\Gamma_D)$. *Find* $(\mathbf{u}, p, T)$ *in* $\mathbf{H}^1(\Omega) \times L^2(\Omega) \times H^1(\Omega)$ *such that* $\mathbf{u}|_{\Gamma_D} = \mathbf{u}_D$ *and* $T|_{\Gamma_D} = T_D$ *solution of*:

$$\mathbf{a}_T(\mathbf{u}, \mathbf{v}) + \mathbf{b}(\mathbf{u}, \mathbf{u}, \mathbf{v}) - (\operatorname{div} \mathbf{v}, p)_{0,\Omega} = \left( \frac{Gr}{Re^2} T \mathbf{k}, \mathbf{v} \right)_{0,\Omega} + (\mathbf{F}, \mathbf{v})_{0,\Omega} \quad \forall \mathbf{v} \in \mathbf{H}^1_{0,\Gamma_D}(\Omega) \tag{14}$$

$$(\operatorname{div} \mathbf{u}, q)_{0,\Omega} = 0 \quad \forall q \in L^2(\Omega) \tag{15}$$

$$a_T(T, \varphi) + b(\mathbf{u}, T, \varphi) = 0 \quad \forall \varphi \in H^1_{0,\Gamma_D}(\Omega) \tag{16}$$

where

$$\mathbf{a}_T(\mathbf{u}, \mathbf{v}) = \int_\Omega \frac{1}{Re} \mu(T) D(\mathbf{u}) : \nabla \mathbf{v} \tag{17}$$

$$\mathbf{b}(\mathbf{u}, \mathbf{v}, \mathbf{w}) = \int_\Omega (\mathbf{u} \cdot \nabla)\mathbf{v} \ \cdot \mathbf{w} \tag{18}$$

$$a_T(\psi, \varphi) = \int_\Omega \frac{1}{Pe} \kappa(T) \nabla \psi \cdot \nabla \varphi \tag{19}$$

$$b(\mathbf{u}, \psi, \varphi) = \int_\Omega (\mathbf{u} \cdot \nabla)\psi \, \varphi \tag{20}$$



DOI: 10.1002/fld

The notations in equations (14)–(20) are inspired by the early work of Duvaut and Lions [21], who analysed the viscosity coupling problem for a Bingham fluid. The index of the applications $\mathbf{a}_T$ and $a_T$ have a mission of showing the temperature field which is associated with the functions of viscosity and conductivity. We note in particular that the expression $a_T(T, \varphi)$ in Equation (16) makes this equation non-linear.

As noted first by Heywood *et al.* [2], existence analysis of steady, constant-property Navier–Stokes problem involving 'do nothing' BCs is a very difficult task. Thus, the variable-property model was analysed here by following an alternative variational formulation first proposed by Bruneau and Fabrie (see [22]) for the constant-property, non-buoyant Navier–Stokes equations.

The alternative variational problem proposed and analysed in the first part is as follows: *Find* $(\mathbf{u}, p, T)$ *in* $\mathbf{H}^1(\Omega) \times L^2(\Omega) \times H^1(\Omega)$, *with* $\mathbf{u} = \mathbf{u}_D$, $T = T_D$ *on* $\Gamma_D$, *solution of*:

$$\mathbf{a}_T(\mathbf{u}, \mathbf{v}) + \tilde{\mathbf{b}}(\mathbf{u}, \mathbf{u}, \mathbf{v}) - (\operatorname{div} \mathbf{v}, p) = \left( \frac{Gr}{Re^2} T\mathbf{k} + \mathbf{F}, \mathbf{v} \right) \quad \forall \mathbf{v} \in \mathbf{H}^1_{0,\Gamma_D}(\Omega) \tag{21}$$

$$(\operatorname{div}, \mathbf{u}, q) = 0 \quad \forall q \in L^2(\Omega) \tag{22}$$

$$a_T(T, \varphi) + \tilde{b}(\mathbf{u}, T, \varphi) = 0 \quad \forall \varphi \in H^1_{0,\Gamma_D}(\Omega) \tag{23}$$

In (21) and (23), the 'convective' forms $\tilde{\mathbf{b}}$ and $\tilde{b}$ are defined by

$$\tilde{\mathbf{b}}(\mathbf{u}, \mathbf{v}, \mathbf{w}) = \mathbf{b}(\mathbf{u}, \mathbf{v}, \mathbf{w}) + \frac{1}{2} \int_{\Gamma_N} [\mathbf{u} \cdot \mathbf{n}]^- \mathbf{v} \cdot \mathbf{w} \tag{24}$$

$$\tilde{b}(\mathbf{u}, \phi, \varphi) = b(\mathbf{u}, \phi, \varphi) + \frac{1}{2} \int_{\Gamma_N} [\mathbf{u} \cdot \mathbf{n}]^- \phi\varphi \tag{25}$$

In (24) and (25), $\mathbf{n}$ refers to the unit outward vector to $\Gamma_N$ and $[\cdot]^-$ refers to the 'negative part' function, defined by $[f]^-(x) = \sup\{-f(x), 0\}$. We also define the 'positive part' function as $[f]^+(x) = \sup\{0, f(x)\}$.

That is, some flux condition on the outflow boundary is introduced into the variational formulation.

We note that a sufficiently regular solution $(\mathbf{u}, p, T)$ of (21)–(23) is also a solution of:

$$-\frac{1}{Re} \nabla \cdot (\mu(T) D(\mathbf{u})) + \mathbf{u} \cdot \nabla \mathbf{u} + \nabla p = \frac{Gr}{Re^2} T\mathbf{k} + \mathbf{F} \tag{26}$$

$$\nabla \cdot \mathbf{u} = 0 \tag{27}$$

$$\mathbf{u} \cdot \nabla T - \frac{1}{Pe} \nabla \cdot (\kappa(T) \nabla T) = 0 \tag{28}$$

$$T = T_D \text{ on } \Gamma_D, \quad \kappa(T) \nabla T \cdot \mathbf{n} + \tfrac{1}{2} [\mathbf{u} \cdot \mathbf{n}]^- T = 0 \text{ on } \Gamma_N \tag{29}$$

$$\mathbf{u} = \mathbf{u}_D \text{ on } \Gamma_D, \quad \boldsymbol{\sigma}(\mathbf{u}, p)(T) : \mathbf{n} + \tfrac{1}{2} [\mathbf{u} \cdot \mathbf{n}]^- \mathbf{u} = \mathbf{0} \text{ on } \Gamma_N \tag{30}$$

Thus, if the resulting velocity field $\mathbf{u}$ is such that $\mathbf{u} \cdot \mathbf{n} \geqslant 0$ on $\Gamma_N$, a behaviour which is admissible for small Reynolds and small buoyant forces, then the solution of problem (21)–(23) is also a solution of (14)–(16) and BCs (6)–(7). This is an important issue, because a solution of Equations (14)–(16) and BCs (6)–(7) is, at least formally, a solution of the steady problem (2)–(4).



DOI: 10.1002/fld

If $\mathbf{u} \cdot \mathbf{n} \leqslant 0$ (re-entrant flow case), then both the problems (21)–(23) and (14)–(16) are no longer equivalent, and, in the authors' knowledge, remains an open problem.

In Part I, the existence and uniqueness of these two uncoupled problems (Navier–Stokes and energy) were proved, with the uniqueness of the Navier–Stokes equations being guaranteed under small data conditions (see Theorems 4.1 and 4.2 of [19]). The existence of a solution for the original coupled problem was established by means of a Picard fixed point strategy, by choosing a temperature $\hat{T}$ for the uncoupling which gives rise to 'frozen' thermophysical coefficients in each iteration.

Because of the buoyancy term, an additional hypothesis was stated in order to have a uniform estimate for the velocity solutions. Denoting by $Z : \hat{T} \mapsto Z_{\hat{T}}$ the application that defines, for each temperature field $\hat{T}$, an operator $Z_{\hat{T}}$ is as follows:

$$\begin{gathered} Z_{\hat{T}} : \mathbf{H}^1(\Omega) \to H^1(\Omega) \\ \mathbf{u} \mapsto Z_{\hat{T}}(\mathbf{u}) = \text{Unique solution of the linearized energy equation (23)} \\ \text{for a given solenoidal velocity field } \mathbf{u} \end{gathered} \tag{31}$$

we will consider as an hypothesis that their inverse application is continuous, an assumption that yields $\|S(\hat{T})\|_{1,\Omega} \leqslant C \|Z_{\hat{T}}(S(\hat{T}))\|_{1,\Omega}$, with $S(\hat{T})$ being the (unique) velocity solution of the $\hat{T}$-uncoupled Navier–Stokes equations. This hypothesis is not unrealistic if we are interested on moderate Reynolds numbers. In Part I, it is shown that this sequence of Picard iterations converges to the solution of the non-linear problem. More details can be found in [19].

## 3. MATHEMATICAL ANALYSIS OF THE DISCRETE PROBLEM

The main part of this article is devoted to the numerical approximation of the coupled problem whose main characteristics and notations were presented in the companion paper [19]. The discretization will be realized by the FE method (FEM). For a detailed explanation on the use of FEM for the Navier–Stokes equations, we refer to [23].

As in the variational formulations presented in the previous section, we have worked with the deformation tensor $D(\mathbf{u})$. We shall perform the analysis for *conforming* FE subspaces: discrete variational formulations with the deformation tensor have some technical difficulties with non-conforming FE regarding, for instance, Korn's inequality (see, for instance, [24]).

We recall the variational problem to be discretized: *Find* $(\mathbf{u}, p, T) \in \mathbf{H}^1(\Omega) \times L^2(\Omega) \times H^1(\Omega)$ *with* $\mathbf{u} = \mathbf{u}_\mathrm{D}$ *and* $T = T_\mathrm{D}$ *on* $\Gamma_\mathrm{D}$ *such that*:

$$\mathbf{a}_T(\mathbf{u}, \mathbf{v}) + \tilde{\mathbf{b}}(\mathbf{u}, \mathbf{u}, \mathbf{v}) - (\operatorname{div} \mathbf{v}, p) = \left( \frac{Gr}{Re^2} T\mathbf{k} + \mathbf{F}, \mathbf{v} \right) \quad \forall \mathbf{v} \in \mathbf{H}^1_{0,\Gamma_\mathrm{D}}(\Omega) \tag{32}$$

$$(\operatorname{div}, \mathbf{u}, q) = 0 \quad \forall q \in L^2(\Omega) \tag{33}$$

$$a_T(T, \varphi) + \tilde{b}(\mathbf{u}, T, \varphi) = 0 \quad \forall \varphi \in H^1_{0,\Gamma_\mathrm{D}}(\Omega) \tag{34}$$

### *3.1. Finite element analysis*

For the sake of simplicity, we develop the analysis by considering that the discrete domain $\Omega_h$ coincides with the continuous domain $\Omega$, here supposed to be polygonal.



DOI: 10.1002/fld

Also, for comparison purposes with other references, we adopt similar notations for the continuity constants utilized in the works of [5, 18], which analysed the standard Boussinesq model. Thus, we shall from now on denote $C^{\mathbf{a}}$, $C^a$, $C^{\mathbf{b}}$, $C^b$ as the continuity constants of $\mathbf{a}_T(\cdot,\cdot)$, $a_T(\cdot,\cdot)$, $\mathbf{b}(\cdot,\cdot,\cdot)$ and $b(\cdot,\cdot,\cdot)$, respectively. Furthermore, we denote by $C^{\mathrm{div}}$ and $C^g$ the continuity constants of the applications $(\operatorname{div}\mathbf{v}, q)$ and $(T\mathbf{k}, \mathbf{v})$, that is, for instance:

$$\begin{aligned} \mathbf{b}(\mathbf{u},\mathbf{v},\mathbf{w}) &\leqslant C^{\mathbf{b}}\|\mathbf{u}\|_{1,\Omega}\|\mathbf{v}\|_{1,\Omega}\|\mathbf{w}\|_{1,\Omega} \\ (\operatorname{div}\mathbf{v}, q) &\leqslant C^{\mathrm{div}}\|\mathbf{v}\|_{1,\Omega}\|q\|_{0,\Omega} \end{aligned} \tag{35}$$

Finally, we denote the constants of Korn's inequality as follows:

$$C^k\|\mathbf{u}\|_{1,\Omega} \leqslant \|D(\mathbf{u})\|_{0,\Omega} \leqslant C^K\|\mathbf{u}\|_{1,\Omega} \tag{36}$$

Let $h>0$ be the mesh discretization parameter, destined to tend towards zero. Let us consider finite-dimensional subspaces parameterized by $h$: $\mathbf{X}^h \subset \mathbf{H}^1(\Omega)$, $Y^h \subset H^1(\Omega)$ and $M^h \subset L^2(\Omega)$. We write the spaces used in the previous section in a classical fashion:

$$\begin{aligned} \mathbf{X}_0^h &= \mathbf{X}^h \cap \mathbf{X}_0, \qquad \mathbf{X}_0 = \mathbf{H}^1_{0,\Gamma_{\mathrm{D}}}(\Omega) \\ Y_0^h &= Y^h \cap Y_0, \quad Y_0 = H^1_{0,\Gamma_{\mathrm{D}}}(\Omega) \end{aligned} \tag{37}$$

Both $\mathbf{X}^h$ and $Y^h$ are Hilbert spaces with the $H^1$-norm, and the homogeneous discrete spaces $\mathbf{X}_0^h$ and $Y_0^h$ are also Hilbert spaces with the gradient (semi-)norm. We keep the $L^2$-norm for $M^h$.

We recall the compact embedding of $\mathbf{H}^1_{0,\Gamma_{\mathrm{D}}}(\Omega)$ into $\mathbf{L}^4(\Omega)$ and of the trace mapping from $\mathbf{H}^1_{0,\Gamma_{\mathrm{D}}}(\Omega)$ onto $\mathbf{L}^3(\Gamma_{\mathrm{N}})$ for each $\mathbf{v}$ in $\mathbf{H}^1_{0,\Gamma_{\mathrm{D}}}(\Omega)$ (see [25]).

Before any further hypothesis, we shall assume the following standard interpolation properties for the discrete spaces: for an integer $m \geqslant 1$, and a generic constant $C$

$$\inf_{\mathbf{v}_h \in \mathbf{X}^h} \|\mathbf{v}-\mathbf{v}_h\|_{1,\Omega} \leqslant Ch^m\|\mathbf{v}\|_{m+1,\Omega} \quad \forall \mathbf{v} \in \mathbf{H}^{m+1}(\Omega) \tag{38}$$

$$\inf_{q_h \in M^h} \|q-q_h\|_{0,\Omega} \leqslant Ch^m\|q\|_{m,\Omega} \quad \forall q \in H^m(\Omega) \tag{39}$$

$$\inf_{\varphi_h \in Y^h} \|\varphi-\varphi_h\|_{1,\Omega} \leqslant Ch^m\|\varphi\|_{m+1,\Omega} \quad \forall \varphi \in H^{m+1}(\Omega) \tag{40}$$

We shall also admit a *compatibility condition* between the discrete velocity and pressure spaces $\mathbf{X}^h$ and $M^h$ by assuming that there exists a positive constant $\beta>0$ such that

$$\inf_{q_h \in M^h} \sup_{\mathbf{v}_h \in \mathbf{X}^h} \frac{\int q_h \operatorname{div}\mathbf{v}_h}{\|\nabla\mathbf{v}_h\|_{0,\Omega}\|q_h\|_{0,\Omega}} \geqslant \beta \tag{41}$$

a property which is equivalent to:

$$\sup_{\mathbf{v}_h \in \mathbf{X}^h} \frac{\int q_h \operatorname{div}\mathbf{v}_h}{\|\nabla\mathbf{v}_h\|_{0,\Omega}} \geqslant \beta\|q_h\|_{0,\Omega} \quad \forall q_h \in M^h \tag{42}$$



DOI: 10.1002/fld

or again,

$$\begin{aligned} &\forall q_h \in M^h, \quad \exists \mathbf{v}_h \in \mathbf{X}^h \text{ such that} \\ &(q_h, \operatorname{div} \mathbf{v}_h) = \|q_h\|_{0,\Omega}^2 \\ &\|\nabla \mathbf{v}_h\|_{0,\Omega} \leqslant C \|q_h\|_{0,\Omega}^2 \end{aligned} \tag{43}$$

Classic pairs of FE families for velocity and pressure verifying (38)–(41) can be found in [26, 27, 23].

We will also consider the subspaces $\mathbf{V}$ and $\mathbf{V}^h$ defined by

$$\begin{aligned} \mathbf{V} &= \{\mathbf{v} \in \mathbf{X}_0, (\operatorname{div} \mathbf{v}, q) = 0, \forall q \in L^2(\Omega)\} \\ \mathbf{V}^h &= \{\mathbf{v}_h \in \mathbf{X}_0^h, (\operatorname{div} \mathbf{v}_h, q_h) = 0, \forall q_h \in M^h\} \end{aligned} \tag{44}$$

We recall that, in general, the inclusion $\mathbf{V}^h \subset \mathbf{V}$ is not valid. The following affine subspaces are also necessary in the sequel:

$$\begin{aligned} \mathbf{X}_1^h &= \{\mathbf{v}_h \in \mathbf{X}^h, \mathbf{v}_h|_{\Gamma_D} = \mathbf{u}_D^h\} \\ \mathbf{X}_2^h &= \{\mathbf{v}_h \in \mathbf{X}_1^h, (\operatorname{div} \mathbf{v}_h, q_h) = 0, \forall q_h \in M^h\} \\ Y_1^h &= \{\varphi_h \in Y^h, \varphi_h|_{\Gamma_D} = T_D^h\} \end{aligned} \tag{45}$$

That is, in (44) we keep only the divergence-free conditions (continuous and discrete, respectively), and in (45) we put, in addition, the non-homogeneous BCs in the space $\mathbf{X}_2^h$. Under compatibility condition (41), this last space is related to $\mathbf{X}_1^h$, the space with only the non-homogeneous BCs, by (see [28, Theorem I.3.3]):

$$\inf_{\mathbf{v}_h \in \mathbf{X}_2^h} \|\mathbf{u} - \mathbf{v}_h\| \leqslant C \inf_{\mathbf{v}_h \in \mathbf{X}_1^h} \|\mathbf{u} - \mathbf{v}_h\| \tag{46}$$

Concerning the discrete representation of the Dirichlet BCs, we shall assume that the discrete BCs are independent of the lifting considered (but the discrete lifting will depend on the continuous one). We can therefore consider a discrete lifting $\mathbf{u}_h^*$ and $T_h^*$ of the (discrete) Dirichlet BCs by means of:

$$\mathbf{u}_h^* = \Pi_h \mathbf{u}^* \quad \text{and} \quad T_h^* = \Pi_h T^*$$

having that $\mathbf{u}_h^* = \mathbf{u}^*$ and $T_h^* = T^*$ on $\Gamma_D$.

With all these considerations and the geometry assumptions considered at the beginning of this section, the following result is a simple consequence of Theorems 4.1 and 4.2 of Part I (see [19]), adapted for the conforming subspace approximation.

*Proposition 3.1*

Let $\mathbf{F} \in \mathbf{L}^2(\Omega)$, $\mathbf{u}_D \in \mathbf{H}^{1/2}(\Gamma_D)$, and $T_D \in H^{1/2}(\Gamma_D)$, with $T_1 \leqslant T_D \leqslant T_2$ a.e. and the traces of the Dirichlet data $\mathbf{u}_D$ and $T_D$ belonging to $H^{1/2}(\Gamma_D)$ (that is, $\gamma_0(\mathbf{u}_D^h) \in \mathbf{H}^{1/2}(\Gamma_D)$ and $\gamma_0(T_D^h) \in H^{1/2}(\Gamma_D)$). Under the regularity of the inverse operator defined by (31), the discrete problem (32)–(34) formulated on a conforming, compatible pair of FE admits a solution $(\mathbf{u}_h, p_h, T_h) \in \mathbf{X}_2^h \times M^h \times Y_1^h$. In addition, if the data are regular and small enough, it is unique.



DOI: 10.1002/fld

*Proof*
This is a direct application of the analysis performed in Part I, by considering the discrete BCs and associated liftings $\mathbf{u}_h^*$ and $T_h^*$. □

If the uniqueness of the solutions of the continuous and the discrete problem can be guaranteed, we can proceed to quantify the error between the solution $(\mathbf{u}, p, T) \in \mathbf{H}^1(\Omega) \times L^2(\Omega) \times H^1(\Omega)$ of

$$\mathbf{a}_T(\mathbf{u}, \mathbf{v}) + \tilde{\mathbf{b}}(\mathbf{u}, \mathbf{u}, \mathbf{v}) - (\operatorname{div} \mathbf{v}, p) = \left( \frac{Gr}{Re^2} T\mathbf{k} + \mathbf{F}, \mathbf{v} \right) \quad \forall \mathbf{v} \in \mathbf{H}^1_{0,\Gamma_D}(\Omega) \tag{47}$$

$$(\operatorname{div} \mathbf{u}, q) = 0 \quad \forall q \in L^2(\Omega) \tag{48}$$

$$a_T(T, \varphi) + \tilde{b}(\mathbf{u}, T, \varphi) = 0 \quad \forall \varphi \in H^1_{0,\Gamma_D}(\Omega) \tag{49}$$

and the discrete solution $(\mathbf{u}_h, p_h, T_h) \in \mathbf{X}_2^h \times M^h \times Y_1^h$ of

$$\mathbf{a}_{T_h}(\mathbf{u}_h, \mathbf{v}_h) + \tilde{\mathbf{b}}(\mathbf{u}_h, \mathbf{u}_h, \mathbf{v}_h) - (\operatorname{div} \mathbf{v}_h, p_h) = \left( \frac{Gr}{Re^2} T_h\mathbf{k} + \mathbf{F}, \mathbf{v}_h \right) \quad \forall \mathbf{v} \in \mathbf{X}_0^h \tag{50}$$

$$(\operatorname{div} \mathbf{u}_h, q_h) = 0 \quad \forall q \in M^h \tag{51}$$

$$a_{T_h}(T_h, \varphi_h) + \tilde{b}(\mathbf{u}_h, T_h, \varphi_h) = 0 \quad \forall \varphi_h \in Y_0^h \tag{52}$$

Our main result is the following.

*Theorem 3.1*
Let the pair of velocity/pressure elements verify the discrete compatibility condition (41). Under the hypotheses of Proposition 3.1 and some other conditions for the data stated in the constraints (66) and (70), the following error estimate between the continuous solution of (47)–(49) and the discrete solution of (50)–(52) holds:

$$\begin{aligned} &\|\mathbf{u} - \mathbf{u}_h\|_{1,\Omega} + \|p - p_h\|_{0,\Omega} + \|T - T_h\|_{1,\Omega} \\ &\leqslant C \left( \inf_{\mathbf{v}_h \in \mathbf{X}_1^h} \|\mathbf{u} - \mathbf{v}_h\|_{1,\Omega} + \inf_{\varphi_h \in Y_1^h} \|T - \varphi_h\|_{1,\Omega} + \inf_{q_h \in M^h} \|p - q_h\|_{0,\Omega} \right) \end{aligned} \tag{53}$$

*Proof*
Let $\mathbf{w}_h \in \mathbf{X}_2^h$. Since $(\operatorname{div}(\mathbf{w}_h - \mathbf{u}_h), q_h) = 0 \ \forall q_h \in M^h$, for the solution $\mathbf{u}_h$ of the discrete problem (50), we have that $(\mathbf{w}_h - \mathbf{u}_h) \in \mathbf{V}^h \cap \mathbf{X}_0^h$.

We subtract the discrete and the continuous Navier–Stokes equations (50) and (47), and testing this difference with the (admissible) test function $(\mathbf{w}_h - \mathbf{u}_h)$, we then have:

$$\begin{aligned} &\mathbf{a}_{T_h}(\mathbf{u}_h, \mathbf{w}_h - \mathbf{u}_h) - \mathbf{a}_T(\mathbf{u}, \mathbf{w}_h - \mathbf{u}_h) + \tilde{\mathbf{b}}(\mathbf{u}_h, \mathbf{u}_h, \mathbf{w}_h - \mathbf{u}_h) - \tilde{\mathbf{b}}(\mathbf{u}, \mathbf{u}, \mathbf{w}_h - \mathbf{u}_h) \\ &+ (\operatorname{div}(\mathbf{w}_h - \mathbf{u}_h), p_h) - (\operatorname{div}(\mathbf{w}_h - \mathbf{u}_h), p) = \frac{Gr}{Re^2}((T_h - T)\mathbf{k}, \mathbf{w}_h - \mathbf{u}_h) \end{aligned} \tag{54}$$



DOI: 10.1002/fld

Next, we introduce two additional and arbitrary terms $q_h \in M^h$ and $\mathbf{z} \in \mathbf{V}$. A simple calculation in (54) gives, for all $\mathbf{v}_h \in \mathbf{X}_0^h$:

$$\begin{aligned}
&\mathbf{a}_{T_h}(\mathbf{u}_h, \mathbf{w}_h - \mathbf{u}_h) - \mathbf{a}_T(\mathbf{u}, \mathbf{w}_h - \mathbf{u}_h) + \mathbf{b}(\mathbf{u}_h - \mathbf{u}, \mathbf{u}_h, \mathbf{w}_h - \mathbf{u}_h) \\
&\quad + \mathbf{b}(\mathbf{u}, \mathbf{u}_h - \mathbf{u}, \mathbf{w}_h - \mathbf{u}_h) + \frac{1}{2}\int_{\Gamma_N} [\mathbf{u}_h \cdot \mathbf{n}]^- \mathbf{u}_h \cdot (\mathbf{w}_h - \mathbf{u}_h) - \frac{1}{2}\int_{\Gamma_N} [\mathbf{u} \cdot \mathbf{n}]^- \mathbf{u} \cdot (\mathbf{w}_h - \mathbf{u}_h) \\
&\quad = -(\operatorname{div}(\mathbf{w}_h - \mathbf{u}_h), q_h - p) + \frac{Gr}{Re^2}((T_h - T)\mathbf{k}, \mathbf{w}_h - \mathbf{u}_h)
\end{aligned} \tag{55}$$

In addition, for all $\mathbf{v}_h \in \mathbf{X}_0^h$:

$$\begin{aligned}
\mathbf{b}(\mathbf{u}_h, \mathbf{u}_h, \mathbf{v}_h) - \mathbf{b}(\mathbf{u}, \mathbf{u}, \mathbf{v}_h) &= \mathbf{b}(\mathbf{u}_h - \mathbf{u}, \mathbf{u}_h, \mathbf{v}_h) + \mathbf{b}(\mathbf{u}, \mathbf{u}_h - \mathbf{u}, \mathbf{v}_h) \\
(\operatorname{div}\mathbf{v}_h, p_h) - (\operatorname{div}\mathbf{v}_h, p) &= (\operatorname{div}\mathbf{v}_h, p_h - q_h) + (\operatorname{div}\mathbf{v}_h, q_h - p)
\end{aligned} \tag{56}$$

From (55) we have:

$$\begin{aligned}
&\mathbf{a}_{T_h}(\mathbf{w}_h - \mathbf{u}_h, \mathbf{w}_h - \mathbf{u}_h) - \frac{1}{Re}\int_\Omega (\mu(T_h) - \mu(T)) D(\mathbf{u}) : D(\mathbf{w}_h - \mathbf{u}_h) \\
&\quad - \mathbf{b}(\mathbf{u}_h - \mathbf{u}, \mathbf{u}_h, \mathbf{w}_h - \mathbf{u}_h) - \mathbf{b}(\mathbf{u}, \mathbf{u}_h - \mathbf{u}, \mathbf{w}_h - \mathbf{u}_h) \\
&\quad + \frac{1}{2}\int_{\Gamma_N} [\mathbf{u}_h \cdot \mathbf{n}]^- (\mathbf{u}_h - \mathbf{u}) \cdot (\mathbf{w}_h - \mathbf{u}_h) - \frac{1}{2}\int_{\Gamma_N} [[\mathbf{u}_h \cdot \mathbf{n}]^- - [\mathbf{u} \cdot \mathbf{n}]^-]\mathbf{u} \cdot (\mathbf{w}_h - \mathbf{u}_h) \\
&\quad = (\operatorname{div}(\mathbf{w}_h - \mathbf{u}_h - \mathbf{z}), q_h - p) + \frac{Gr}{Re^2}((T_h - T)\mathbf{k}, \mathbf{w}_h - \mathbf{u}_h) \\
&\qquad + \mathbf{a}_{T_h}(\mathbf{u} - \mathbf{w}_h, \mathbf{w}_h - \mathbf{u}_h)
\end{aligned} \tag{57}$$

The continuity of the applications $a$, $b$, $\mathbf{a}$, $\mathbf{b}$ and those defined in (35) and (36), with the use of Hölder's inequality and the boundedness of the forms $\mathbf{a}_T$ and $a_T$ gives for (57):

$$\begin{aligned}
&\frac{C^k \mu_1}{Re}\|\mathbf{w}_h - \mathbf{u}_h\|_{1,\Omega}^2 - C^{\mathbf{b}}\|\mathbf{u}_h\|_{1,\Omega}\|\mathbf{u}_h - \mathbf{u}\|_{1,\Omega}\|\mathbf{w}_h - \mathbf{u}_h\|_{1,\Omega} \\
&\quad - C^{\mathbf{b}}\|\mathbf{u}\|_{1,\Omega}\|\mathbf{u}_h - \mathbf{u}\|_{1,\Omega}\|\mathbf{w}_h - \mathbf{u}_h\|_{1,\Omega} - C^3\|\mathbf{u}_h\|_{1,\Omega}\|\mathbf{u}_h - \mathbf{u}\|_{1,\Omega}\|\mathbf{w}_h - \mathbf{u}_h\|_{1,\Omega} \\
&\qquad \leqslant C^3\|\mathbf{u}\|_{1,\Omega}\|\mathbf{u}_h - \mathbf{u}\|_{1,\Omega}\|\mathbf{w}_h - \mathbf{u}_h\|_{1,\Omega} + C^{\operatorname{div}}\|\mathbf{w}_h - \mathbf{u}_h - \mathbf{z}\|_{1,\Omega}\|q_h - p\|_{0,\Omega} \\
&\qquad\quad + \frac{Gr}{Re^2}C^g\|T_h - T\|_{1,\Omega}\|\mathbf{w}_h - \mathbf{u}_h\|_{1,\Omega} + C^{\mathbf{a}}\|\mathbf{u} - \mathbf{w}_h\|_{1,\Omega}\|\mathbf{w}_h - \mathbf{u}_h\|_{1,\Omega} \\
&\qquad\quad + \frac{\operatorname{Lip}(\mu)}{Re}C^K\|T_h - T\|_{1,\Omega}\|\mathbf{u}\|_{1,\Omega}\|\mathbf{w}_h - \mathbf{u}_h\|_{1,\Omega}
\end{aligned} \tag{58}$$

In (58) and hereafter, $\operatorname{Lip}(\mu)$ and $\operatorname{Lip}(\kappa)$ are the Lipschitz-continuity constants of the dynamical viscosity and the thermal conductivity functions.



DOI: 10.1002/fld

If $\mathbf{w}_h = \mathbf{u}_h$, (58) is trivially verified. If such is not the case, Equation (58) can be divided by $\|\mathbf{w}_h - \mathbf{u}_h\|_{1,\Omega}$. An adequate grouping of the terms yields:

$$\frac{C^k \mu_1}{Re}\|\mathbf{w}_h - \mathbf{u}_h\|_{1,\Omega} \leqslant (C^{\mathbf{b}} + C^3)\|\mathbf{u}_h - \mathbf{u}\|_{1,\Omega}(\|\mathbf{u}\|_{1,\Omega} + \|\mathbf{u}_h\|_{1,\Omega}) + C^{\mathrm{div}}\frac{\|\mathbf{w}_h - \mathbf{u}_h - \mathbf{z}\|_{1,\Omega}\|q_h - p\|_{0,\Omega}}{\|\mathbf{w}_h - \mathbf{u}_h\|_{1,\Omega}} + \frac{\mathrm{Lip}(\mu)}{Re}C^K\|T_h - T\|_{1,\Omega}\|\mathbf{u}\|_{1,\Omega} + \frac{Gr}{Re^2}C^g\|T_h - T\|_{1,\Omega} + C^K\|\mathbf{u} - \mathbf{w}_h\|_{1,\Omega} \tag{59}$$

At this level, the choice of $\mathbf{z} \in \mathbf{V}$ being arbitrary, we take in particular $\mathbf{z} = \mathbf{0}$ and (59) becomes:

$$\frac{C^k \mu_1}{Re}\|\mathbf{w}_h - \mathbf{u}_h\|_{1,\Omega} \leqslant (C^{\mathbf{b}} + C^3)\|\mathbf{u}_h - \mathbf{u}\|_{1,\Omega}(\|\mathbf{u}\|_{1,\Omega} + \|\mathbf{u}_h\|_{1,\Omega}) + C^{\mathrm{div}}\|q_h - p\|_{0,\Omega} + \frac{\mathrm{Lip}(\mu)}{Re}C^K\|T_h - T\|_{1,\Omega}\|\mathbf{u}\|_{1,\Omega} + \frac{Gr}{Re^2}C^g\|T_h - T\|_{1,\Omega} + C^{\mathbf{a}}\|\mathbf{u} - \mathbf{w}_h\|_{1,\Omega} \tag{60}$$

We recognize the term associated with the temperature $\|T - T_h\|$ in estimation (60). The next step is to obtain a bound for this term from the energy equation in terms of the approximations of $\mathbf{u}_h$ and $T_h$. For this, we subtract the discrete and the continuous energy equations (52) and (49) and we obtain:

$$a_T(T, \varphi_h) - a_{T_h}(T_h, \varphi_h) + \tilde{b}(\mathbf{u}, T, \varphi_h) - \tilde{b}(\mathbf{u}_h, T_h, \varphi_h) = 0 \tag{61}$$

or, by adding $a_{T_h}(T, \varphi_h)$:

$$a_{T_h}(T - T_h, \varphi_h) + \frac{1}{Pe}\int_\Omega (\kappa(T) - \kappa(T_h))\nabla T \nabla \varphi_h + \tilde{b}(\mathbf{u}, T, \varphi_h) - \tilde{b}(\mathbf{u}_h, T_h, \varphi_h) = 0 \tag{62}$$

Let $S_h \in Y_1^h$ be arbitrary. We choose as test function: $\varphi_h = S_h - T_h$. The addition to both sides of (61) of the term $b(\mathbf{u}_h, S_h, S_h - T_h) - b(\mathbf{u}, T, S_h - T_h)$ gives:

$$a_{T_h}(S_h - T_h, S_h - T_h) + b(\mathbf{u}_h, S_h - T_h, S_h - T_h) = a_{T_h}(S_h - T, S_h - T_h) + b(\mathbf{u}_h, S_h, S_h - T_h) - b(\mathbf{u}, T, S_h - T_h) + \frac{1}{Pe}\int_\Omega (\kappa(T) - \kappa(T_h))\nabla T \nabla (S_h - T_h) - \frac{1}{2}\int_{\Gamma_N} [\mathbf{u}\cdot\mathbf{n}]^-(T - T_h)(S_h - T_h) - \frac{1}{2}\int_{\Gamma_N} ([\mathbf{u}\cdot\mathbf{n}]^- - [\mathbf{u}_h\cdot\mathbf{n}]^-)T_h(S_h - T_h) \tag{63}$$

We conveniently introduce an arbitrary velocity term $\mathbf{w}_h$ in this estimate, and (63) becomes:

$$a_{T_h}(S_h - T_h, S_h - T_h) + b(\mathbf{u}_h, S_h - T_h, S_h - T_h) = a_{T_h}(S_h - T, S_h - T_h) + b(\mathbf{w}_h - \mathbf{u}, T, S_h - T_h) + b(\mathbf{u}_h, S_h - T, S_h - T_h) - b(\mathbf{w}_h - \mathbf{u}_h, T, S_h - T_h)$$



DOI: 10.1002/fld

$$+\frac{1}{Pe}\int_\Omega(\kappa(T)-\kappa(T_h))\nabla T\nabla(T_h-S_h)$$
$$-\frac{1}{2}\int_{\Gamma_N}[\mathbf{u}\cdot\mathbf{n}]^-(T-T_h)(S_h-T_h)-\frac{1}{2}\int_{\Gamma_N}([\mathbf{u}\cdot\mathbf{n}]^--[\mathbf{u}_h\cdot\mathbf{n}]^-)T_h(S_h-T_h) \quad (64)$$

We proceed to estimate the above equation in terms of the norms. As for the Navier–Stokes estimate (58), this time we obtain from (64):

$$\left(C^3\frac{\kappa_1}{Pe}-C^b\|\mathbf{u}_h\|_{1,\Omega}\right)\|S_h-T_h\|_{1,\Omega}\leqslant C^a\|S_h-T\|_{1,\Omega}+C^b\|\mathbf{w}_h-\mathbf{u}\|_{1,\Omega}\|T\|_{1,\Omega}$$
$$+C^b\|\mathbf{u}_h\|_{1,\Omega}\|S_h-T\|_{1,\Omega}+C^b\|\mathbf{w}_h-\mathbf{u}_h\|_{1,\Omega}\|T\|_{1,\Omega}+\frac{\mathrm{Lip}(\kappa)}{Pe}\|T-T_h\|_{1,\Omega}\|T\|_{1,\Omega}$$
$$+C^6\|\mathbf{u}\|_{1,\Omega}\|T-T_h\|_{1,\Omega}+C^7\|\mathbf{u}-\mathbf{u}_h\|_{1,\Omega}\|T_h\|_{1,\Omega} \quad (65)$$

And, from the triangular inequality:

$$\|T-T_h\|_{1,\Omega}\leqslant\|T-S_h\|_{1,\Omega}+\|S_h-T_h\|_{1,\Omega}$$
$$\leqslant\|T-S_h\|_{1,\Omega}+Pe(C^3\kappa_1-C^b\|\mathbf{u}_h\|_{1,\Omega}Pe)^{-1}\Big[C^a\|S_h-T\|_{1,\Omega}+C^b\|\mathbf{w}_h-\mathbf{u}\|_{1,\Omega}\|T\|_{1,\Omega}$$
$$+C^b\|\mathbf{u}_h\|_{1,\Omega}\|S_h-T\|_{1,\Omega}+C^b\|\mathbf{w}_h-\mathbf{u}_h\|_{1,\Omega}\|T\|_{1,\Omega}+\frac{\mathrm{Lip}(\kappa)}{Pe}\|T-T_h\|_{1,\Omega}\|T\|_{1,\Omega}$$
$$+C^6\|\mathbf{u}\|_{1,\Omega}\|T-T_h\|_{1,\Omega}+C^7\|\mathbf{u}-\mathbf{u}_h\|_{1,\Omega}\|T_h\|_{1,\Omega}\Big] \quad (66)$$

If we define the constant $\mathscr{C}_1$ by

$$\mathscr{C}_1:=\left(1-Pe(C^3\kappa_1-C^b\|\mathbf{u}_h\|_{1,\Omega}Pe)^{-1}\left(\frac{1}{Pe}\mathrm{Lip}(\kappa)\|T\|_{1,\Omega}+C^6\|\mathbf{u}\|_{1,\Omega}\right)\right)^{-1}$$

we observe that this constant is positive for small temperature data. From (66), we obtain:

$$\|T-T_h\|_{1,\Omega}\leqslant\mathscr{C}_1\Big[1+Pe(C^3\kappa_1-C^b\|\mathbf{u}_h\|_{1,\Omega}Pe)^{-1}(C^a+C^b\|\mathbf{u}_h\|_{1,\Omega}\|S_h-T\|_{1,\Omega}$$
$$+C^b\|T\|_{1,\Omega}(\|\mathbf{w}_h-\mathbf{u}\|_{1,\Omega}+\|\mathbf{w}_h-\mathbf{u}_h\|_{1,\Omega})+C^7\|\mathbf{u}-\mathbf{u}_h\|_{1,\Omega}\|T_h\|_{1,\Omega}\Big] \quad (67)$$

Using (67), we come back to the Navier–Stokes estimation obtained in (60), and we obtain

$$\frac{C^k\mu_1}{Re}\|\mathbf{w}_h-\mathbf{u}_h\|_{1,\Omega}\leqslant(C^{\mathbf{b}}+C^3)\|\mathbf{u}_h-\mathbf{u}\|_{1,\Omega}(\|\mathbf{u}_h\|_{1,\Omega}+\|\mathbf{u}\|_{1,\Omega})+C^{\mathrm{div}}\|q_h-p\|_{0,\Omega}$$
$$+\mathscr{C}_2[(1+Pe(C^3\kappa_1-C^b\|\mathbf{u}_h\|_{1,\Omega}Pe)^{-1}(C^{\mathbf{a}}+C^b\|\mathbf{u}_h\|_{1,\Omega})]\|S_h-T\|_{1,\Omega}$$
$$+\mathscr{C}_2[C^b\|T\|_{1,\Omega}(\|\mathbf{w}_h-\mathbf{u}\|_{1,\Omega}+\|\mathbf{w}_h-\mathbf{u}_h\|_{1,\Omega})$$
$$+C^7\|\mathbf{u}-\mathbf{u}_h\|_{1,\Omega}\|T_h\|_{1,\Omega}]+C^{\mathbf{a}}\|\mathbf{u}-\mathbf{w}_h\|_{1,\Omega} \quad (68)$$



DOI: 10.1002/fld

where the positive constant $\mathscr{C}_2$ is defined by

$$\mathscr{C}_2 = \mathscr{C}_1 \left( \frac{1}{Re} \mathrm{Lip}(\mu) C^k \|\mathbf{u}\|_{1,\Omega} + \frac{Gr}{Re^2} \right)$$

After grouping similar terms, we have

$$\mathscr{C}_3 \|\mathbf{w}_h - \mathbf{u}_h\|_{1,\Omega} \leqslant \mathscr{C}_4 \|\mathbf{w}_h - \mathbf{u}\|_{1,\Omega} + \mathscr{C}_5 \|S_h - T\|_{1,\Omega} + C^{\mathrm{div}} \|q_h - p\|_{0,\Omega} \tag{69}$$

with real constants $\mathscr{C}_3, \mathscr{C}_4, \mathscr{C}_5$ defined by

$$\mathscr{C}_3 = \left[ \frac{C^k \mu_1}{Re} - \mathscr{C}_2 C^b \|T\|_{1,\Omega} - ((C^b + C^3)(\|\mathbf{u}_h\|_{1,\Omega} - \|\mathbf{u}\|_{1,\Omega}) + \mathscr{C}_2 C^7 \|T_h\|_{1,\Omega}) \right] \tag{70}$$

$$\mathscr{C}_4 = [C^{\mathbf{a}} + \mathscr{C}_2 C^b \|T\|_{1,\Omega} + ((C^b + C^3)(\|\mathbf{u}_h\|_{1,\Omega} - \|\mathbf{u}\|_{1,\Omega}) + \mathscr{C}_2 C^7 \|T_h\|_{1,\Omega}] \tag{71}$$

$$\mathscr{C}_5 = [\mathscr{C}_2 [1 + Pe(C^3 \kappa_1 - C^{\mathbf{b}} \|\mathbf{u}_h\|_{1,\Omega} Pe)^{-1} [(C^{\mathbf{a}} + C^{\mathbf{b}} \|\mathbf{u}_h\|_{1,\Omega})] \tag{72}$$

The real constant $\mathscr{C}_3$ is positive under the hypothesis of small data (low velocities and temperature, moderate buoyant force). The constants $\mathscr{C}_4$ and $\mathscr{C}_5$ are positive by definition. As the velocity and temperature solutions $\|\mathbf{u}\|_{1,\Omega}$, $\|\mathbf{u}_h\|_{1,\Omega}$, $\|T\|_{1,\Omega}$ and $\|T_h\|_{1,\Omega}$ are bounded by the data, these three constants defined by (70)–(72) are also bounded.

Under the condition imposed by (70) requiring that $\mathscr{C}_2 > 0$, we obtain a bound for $\|\mathbf{w}_h - \mathbf{u}_h\|_{1,\Omega}$ in (69) in terms of $\|\mathbf{w}_h - \mathbf{u}\|_{1,\Omega}$, $\|S_h - T\|_{1,\Omega}$ and $\|p - q_h\|_{0,\Omega}$. Next, triangular inequality and (70) results in:

$$\begin{aligned} \|\mathbf{u} - \mathbf{u}_h\|_{1,\Omega} &\leqslant \|\mathbf{u} - \mathbf{w}_h\|_{1,\Omega} + \|\mathbf{w}_h - \mathbf{u}_h\|_{1,\Omega} \\ &\leqslant \frac{1 + \mathscr{C}_4}{\mathscr{C}_3} \|\mathbf{u} - \mathbf{w}_h\|_{1,\Omega} + \frac{\mathscr{C}_5}{\mathscr{C}_3} \|T - S_h\|_{1,\Omega} + \frac{C^{\mathrm{div}}}{\mathscr{C}_3} \|q_h - p\|_{0,\Omega} \end{aligned} \tag{73}$$

The choice for the elements $\mathbf{w}_h$, $S_h$, $q_h$ being arbitrary, we can state from (73)

$$\begin{aligned} \|\mathbf{u} - \mathbf{u}_h\|_{1,\Omega} \leqslant \frac{1 + \mathscr{C}_4}{\mathscr{C}_3} \inf_{\mathbf{w}_h \in \mathbf{X}_2^h} \|\mathbf{u} - \mathbf{w}_h\|_{1,\Omega} + \frac{\mathscr{C}_5}{\mathscr{C}_3} \inf_{S_h \in Y_1^h} \|T - S_h\|_{1,\Omega} \\ + \frac{C^{\mathrm{div}}}{\mathscr{C}_3} \inf_{q_h \in M^h} \|p - q_h\|_{0,\Omega} \end{aligned} \tag{74}$$

In (74), the infimum for the velocity approximations is taken in the space $\mathbf{X}_2^h$ (BCs *and* discrete divergence-free conditions). Following (46), with the discrete compatibility condition (41) this infimum is bounded by the infimum of $\mathbf{w}_h \in \mathbf{X}_1^h$ (BCs only), and we obtain the first estimate in (53).

In a similar manner, we can estimate the term $\|T - T_h\|_{1,\Omega}$. Returning to (67) and with the estimations of $\|\mathbf{w}_h - \mathbf{u}_h\|_{1,\Omega}$ and $\|\mathbf{u} - \mathbf{u}_h\|_{1,\Omega}$ given by (69) and (73) we obtain, for other generic constants $\mathscr{C}_6, \mathscr{C}_7, \mathscr{C}_8$ that

$$\|T - T_h\|_{1,\Omega} \leqslant \mathscr{C}_6 \|\mathbf{u} - \mathbf{w}_h\|_{1,\Omega} + \mathscr{C}_7 \|T - S_h\|_{1,\Omega} + \mathscr{C}_8 \|p - q_h\|_{0,\Omega} \tag{75}$$

and the temperature estimate for (53) follows.



DOI: 10.1002/fld

Finally, for the pressure estimate, by considering the Navier–Stokes equations (47) and (50) tested against $\mathbf{v}_h \in \mathbf{X}_0^h$ we obtain

$$\begin{aligned}(\operatorname{div}\mathbf{v},\, p) &= \mathbf{a}_T(\mathbf{u},\mathbf{v}_h) + \tilde{\mathbf{b}}(\mathbf{u},\mathbf{u},\mathbf{v}_h) - \frac{Gr}{Re^2}(T\mathbf{k}+\mathbf{F},\mathbf{v}_h)\\ (\operatorname{div}\mathbf{v}_h,\, p) &= \mathbf{a}_{T_h}(\mathbf{u}_h,\mathbf{v}_h) + \tilde{\mathbf{b}}(\mathbf{u}_h,\mathbf{u}_h,\mathbf{v}_h) - \frac{Gr}{Re^2}(T_h\mathbf{k}+\mathbf{F},\mathbf{v}_h)\end{aligned} \tag{76}$$

Let $q_h \in M^h$. The differences between the two equations in (76) result in

$$\begin{aligned}(\operatorname{div}\mathbf{v}_h, q_h - p_h) = (\operatorname{div}\mathbf{v}_h, q_h - p) - \frac{Gr}{Re^2}((T-T_h)\mathbf{k},\mathbf{v}_h) - \mathbf{a}_{T_h}(\mathbf{u}_h-\mathbf{u},\mathbf{v}_h)\\ \mathbf{b}(\mathbf{u}_h,\mathbf{u}-\mathbf{u}_h,\mathbf{v}_h) + \mathbf{b}(\mathbf{u}-\mathbf{u}_h,\mathbf{u},\mathbf{v}_h) + \frac{1}{Re}\int_\Omega (\mu(T_h)-\mu(T))D(\mathbf{u}):D(\mathbf{v}_h)\\ + \frac{1}{2}\int_{\Gamma_N}[\mathbf{u}_h\cdot\mathbf{n}]^-(\mathbf{u}_h-\mathbf{u})\cdot\mathbf{v}_h - \frac{1}{2}\int_{\Gamma_N}[[\mathbf{u}_h\cdot\mathbf{n}]^- - [\mathbf{u}\cdot\mathbf{n}]^-]\mathbf{u}\cdot\mathbf{v}_h\end{aligned} \tag{77}$$

If we note by $\beta$ the (strictly positive) bound for the uniform compatibility condition (41), as in the previous estimations, we have

$$\begin{aligned}\beta\|\mathbf{v}_h\|_{1,\Omega}\|q_h-p_h\|_{0,\Omega} \leqslant C^{\mathrm{div}}\|\mathbf{v}_h\|_{1,\Omega}\|q_h-p\|_{0,\Omega} + C^g\frac{Gr}{Re^2}\|\mathbf{v}_h\|_{1,\Omega}\|T-T_h\|_{1,\Omega}\\ + C^{\mathbf{a}}\|\mathbf{u}-\mathbf{u}_h\|_{1,\Omega}\|\mathbf{v}_h\|_{1,\Omega} + C^K\frac{\mathrm{Lip}(\mu)}{Re}\|T-T_h\|_{1,\Omega}\|\mathbf{u}\|_{1,\Omega}\|\mathbf{v}_h\|_{1,\Omega}\\ + C^{\mathbf{b}}\|\mathbf{u}_h\|_{1,\Omega}\|\mathbf{u}-\mathbf{u}_h\|_{1,\Omega}\|\mathbf{v}_h\|_{1,\Omega} + C^{\mathbf{b}}\|\mathbf{u}-\mathbf{u}_h\|_{1,\Omega}\|\mathbf{u}\|_{1,\Omega}\|\mathbf{v}_h\|_{1,\Omega}\\ + C^9(\|\mathbf{u}\|_{1,\Omega}+\|\mathbf{u}_h\|_{1,\Omega})\|\mathbf{u}-\mathbf{u}_h\|_{1,\Omega}\|\mathbf{v}_h\|_{1,\Omega}(\|\mathbf{u}\|_{1,\Omega}+\|\mathbf{u}_h\|_{1,\Omega})\end{aligned} \tag{78}$$

If $\mathbf{v}_h = 0$ the estimation above is trivial. If this is not the case, the division by $\beta\|\mathbf{v}_h\|_{1,\Omega}$ results in

$$\begin{aligned}\|q_h-p_h\|_{0,\Omega} \leqslant \frac{C^{\mathrm{div}}}{\beta}\|q_h-p\|_{0,\Omega} + \left(\frac{Gr}{\beta Re^2}C^g + \|\mathbf{u}\|_{1,\Omega}C^K\frac{\mathrm{Lip}(\mu)}{\beta Re}\right)\|T-T_h\|_{1,\Omega}\\ \beta^{-1}(C^{\mathbf{a}} + (C^{\mathbf{b}}+C^9)(\|\mathbf{u}_h\|_{1,\Omega}+\|\mathbf{u}\|_{1,\Omega}))\|\mathbf{u}-\mathbf{u}_h\|_{1,\Omega}\end{aligned} \tag{79}$$

And finally, the triangular inequality leads to

$$\begin{aligned}\|p-p_h\|_{0,\Omega} &\leqslant \|p-q_h\|_{0,\Omega} + \|q_h-p_h\|_{0,\Omega}\\ &\leqslant \left(1+\frac{C^{\mathrm{div}}}{\beta}\right)\|p-q_h\|_{0,\Omega} + \left(\frac{Gr}{\beta Re^2}C^g + \|\mathbf{u}\|_{1,\Omega}C^K\frac{\mathrm{Lip}(\mu)}{\beta Re}\right)\|T-T_h\|_{1,\Omega}\\ &\quad \beta^{-1}(C^{\mathbf{a}} + (C^{\mathbf{b}}+C^9)(\|\mathbf{u}_h\|_{1,\Omega}+\|\mathbf{u}\|_{1,\Omega}))\|\mathbf{u}-\mathbf{u}_h\|_{1,\Omega}\end{aligned} \tag{80}$$



DOI: 10.1002/fld

With the previous estimations obtained for $\|\mathbf{u}-\mathbf{u}_h\|_{1,\Omega}$ and $\|T-T_h\|_{1,\Omega}$ we have the final estimation which gives (53). □

*Remark 1*

As mentioned in Part I (see [19]), from the study realized in this section, it follows that for the model with generalized outflow BCs analysed, if we consider in addition $\alpha, \beta \in \mathbb{R}^+$ and $g \in L^2(\Omega)$, we can adapt the previous FE analysis to the model given by

$$\alpha(\mathbf{u}, \mathbf{v}) + \mathbf{a}_T(\mathbf{u}, \mathbf{v}) + \mathbf{b}(\mathbf{u}, \mathbf{u}, \mathbf{v}) + \frac{1}{2}\int_{\Gamma_N} [\mathbf{u}\cdot\mathbf{n}]^- \mathbf{u}\cdot\mathbf{v} + (\operatorname{div}\mathbf{v}, p) = (\mathbf{F}, \mathbf{v}) + \frac{Gr}{Re^2}(T\mathbf{k}, \mathbf{v})$$
$$(\operatorname{div}\mathbf{u}, \varphi) = 0 \tag{81}$$
$$\beta(T, \psi) + a_T(T, \psi) + b(\mathbf{u}, T, \psi) + \frac{1}{2}\int_{\Gamma_N} [\mathbf{u}\cdot\mathbf{n}]^- T\psi = (g, \psi)$$

All the previous proofs and bounds are easily adapted to this new situation. In consequence, one can show that the discretized version of (81) admits a unique solution when using small data, with newer *a priori* bounds and a new (and weaker) ellipticity condition instead of (9).

This problem (81) arises when the corresponding evolution problem is discretized by backward difference formulas (see [29]).

## 4. NUMERICAL EXPERIMENTS

This section is devoted to the discussion of some numerical experiments performed on the analysis of the coupled steady problem (47)–(49), in view of validating the model in some simple and well-known physical cases.

Because the dynamics of this kind of coupling are expected to be unsteady, we shall also present further unsteady experiments. Although the previous analysis considered the steady problem, following Remark 1, the core of the unsteady code is based on a sequence of augmented steady-type equations.

### *4.1. Main aspects of the FE code*

The numerical code is implemented with the $Q2$–$P1$ pair of FE for the velocity and pressure, a pair of inf–sup compatible FEs. For the temperature, we keep $Q2$ approximations as we do for each component of the velocity field. Therefore, the approximation results deduced in the previous section are applicable.

This choice of the elements is motivated by two fundamental reasons: first, the good and robust behaviour that situates the $Q2$–$P1$ pair as one of the most existing currently for two-dimensional flow calculations (see, for instance, [30–32]), and second, due to the consideration of the buoyancy term in the model. It seems more reasonable to have a discontinuous approximation of pressure in order to assure an element-level mass balance, and also to control the incompressibility condition and the quality of the hydrostatic pressure (see [29, 33]).

As in the previous analysis, we perform in the code a global decoupling with temperature (outer iteration), and we solve the associated Navier–Stokes equations (inner iteration), for this



DOI: 10.1002/fld

temperature field, followed by the resolution of a linear energy equation. The inner iteration of the Navier–Stokes equations is carried out by the Picard iteration, as well as for the outer iteration.

The finite-dimensional system in each resolution step of the Navier–Stokes equations is solved globally (velocity and pressure) by means of an incomplete block LU preconditioning strategy. The resulting preconditioned system is solved iteratively by BICGSTAB(4) (see [34]). Once some relative error bound is reached in two successive approximations for the velocity, the inner iteration ends and we proceed with the resolution of the energy equation with the calculated velocity for the convective term.

The finite-dimensional system in the energy equation is solved by GMRESR (see [35]). The same stopping criterion on the relative error between two successive temperature approximations is used for the global (outer) iteration.

In the following, the geometry for all the numerical experiments corresponds to a two-dimensional straight channel with a 1:10 height/width ratio. The fluid studied is water, with a viscosity law chosen by means of the Andrade correlation valid for [10, 100°C]: $\mu(T) = C_1 \exp^{C_2/T}$, with constants $C_1 = \exp(-12.9896)$ and $C_2 = 1780.622$ obtained by least-squares fitting according to the viscosity values found in the literature (see [36, 37]). The water enters in the channel at a constant velocity and a temperature of 20°C. We first consider the two isothermal walls kept at 80°C with no buoyancy effect, and in the second part a non-isothermal wall with 20°C at the top, and 80°C at the bottom, and with buoyancy effects.

Because of the non-dimensional model, the non-dimensional height and width in the code are 1 and 10, respectively. We then choose as vertical spatial step $h_y = \frac{1}{25}$ and an horizontal step $h_x = \frac{2}{25}$. In the following results, the tolerances for the iterative inner and outer iterations was set to $10^{-6}$. Concerning the solvers, a $10^{-9}$ tolerance was required. The mesh size has been compared and tested against finer meshes, giving similar results which will be presented later.

### *4.2. Steady results: isothermal walls temperature with no buoyancy*

First, if we consider a constant velocity at the inflow, we do not have the regularity profile required in our previous analysis. However, this is a heuristic way to validate the code performances. It is well known that in the laminar steady flow, a uniform velocity profile at the entry becomes a parabola inside the channel (Poiseuille profile). In this first experiment, we do not consider buoyancy effects, and we therefore have $Gr = 0$.

We consider the two cases: a constant value for the viscosity (taken on the reference temperature $T_m$), and secondly the case corresponding to a variable viscosity following the Andrade law $\mu(T) = C_1 \exp^{C_2/T}$, $C_1 = \exp(-12.9896)$, $C_2 = 1780.622$ (see [38]).

We choose $T_m = (T_{\text{upper}} + T_{\text{lower}})/2 = 50°\text{C}$, as the reference temperature, which gives a Prandtl number equal to $Pr_m = 3.57$. The Reynolds number is chosen as $Re_m = 10$. The characteristic temperature difference is $\Delta T_{\text{ref}} = T_{\text{walls}} - T_{\text{inlet}} = 60°\text{C}$, from which the non-dimensional temperature is given by

$$\theta = \frac{T - T_m}{\Delta T_{\text{ref}}}, \quad -0.5 \leqslant \theta \leqslant 0.5 \tag{82}$$

Figure 1 shows the velocity profiles at the section $x = 1$. We note that for the constant viscosity case, the profile obtained is in very good agreement with the well-known Poiseuille profile [39]. For the variable viscosity model, the velocity profile is much more flattened, which is a classical result for liquids [39].



DOI: 10.1002/fld

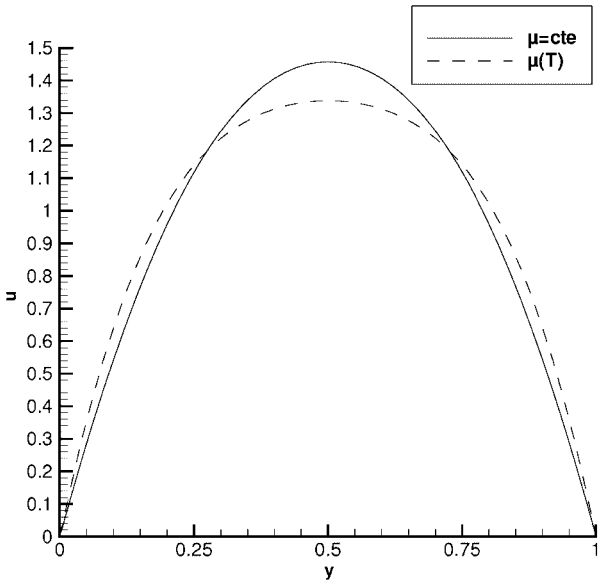


Figure 1. Steady experiment: horizontal velocity profiles at $x = 1$ for the isothermal walls simulation. The continuous line indicates the constant-viscosity simulation, and the dashed line indicates the Andrade-law viscosity liquid simulation.

The local Nusselt number $Nu(x)$ is defined classically by

$$Nu(x) = \frac{\partial\theta/\partial z}{\theta_w - \theta_\mathrm{b}} \tag{83}$$

with $\theta_\mathrm{b}$ the bulk temperature given by:

$$\theta_\mathrm{b} = \int_0^1 u\theta \, \mathrm{d}z \tag{84}$$

Figure 2 shows for both the situations studied a classical behaviour corresponding to a slight increase of heat transfer, taking into account the variation of viscosity with temperature, as can be confirmed in [39]. These results confirm the code validation.

### *4.3. Steady results: non-isothermal wall temperature (buoyancy effects)*

As a second numerical experiment, we keep the entry temperature at 20°C and the lower wall at 80°C. We now fix 20°C for the upper temperature and consider the buoyancy effects.

The reference temperature is kept at $T_m = 50$°C, with an associated Prandtl number $Pr_m = 3.57$. We choose values for $Re_m = 5$ and $Gr_m = 1000$. It is shown in [29], that for these parameters the flow is naturally unsteady with a regular structure of thermoconvective travelling waves associated with the mixed convection. It is worth noting that the fundamental nature of the phenomena is unsteady (streamwise and timewise periodic). Thus, the following results must be understood as qualitative only.



DOI: 10.1002/fld

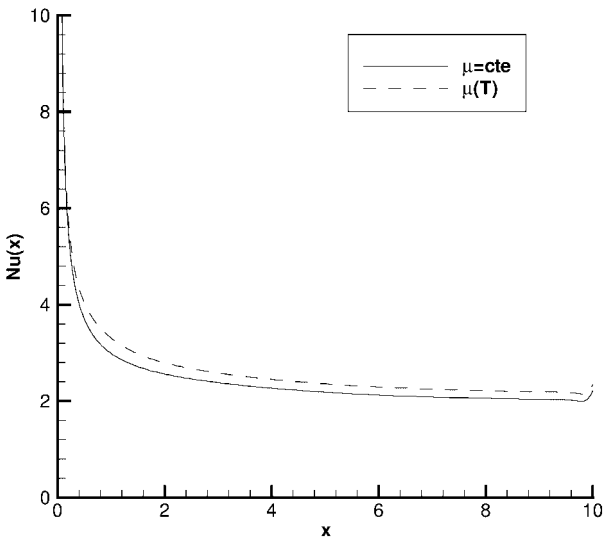


Figure 2. Steady experiment: local Nusselt number distribution $Nu(x)$ on the channel. The continuous line indicates the constant-viscosity simulation, and the dashed line indicates the Andrade-law viscosity liquid simulation.

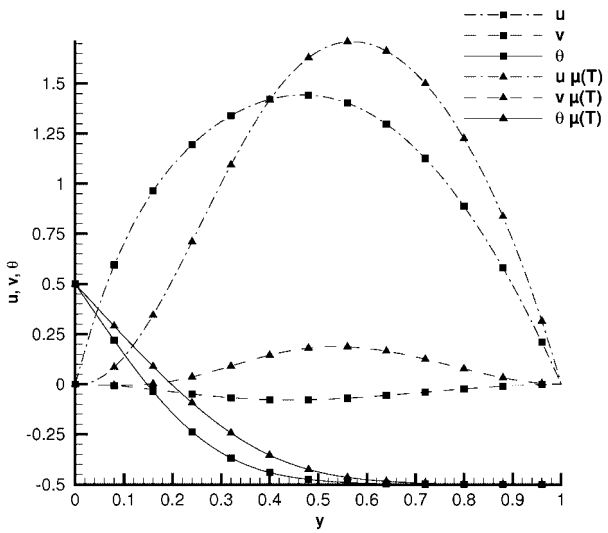


Figure 3. Steady experiment with non-isothermal walls and no buoyancy: the horizontal velocity, radial velocity and temperature profiles are shown at $x = 0.5$, for the non-isothermal walls. The square symbol represents the case $\mu =$ constant. The triangle symbols represents the Andrade-law fluid simulation $\mu = \mu(T)$.

Figure 3 shows the velocity and temperature profiles at $x = 0.5$ for constant viscosity and buoyancy, and for variable viscosity and without buoyancy. We have chosen these two cases in order to compare the effects of these conditions: with and without variable viscosity, with and



DOI: 10.1002/fld

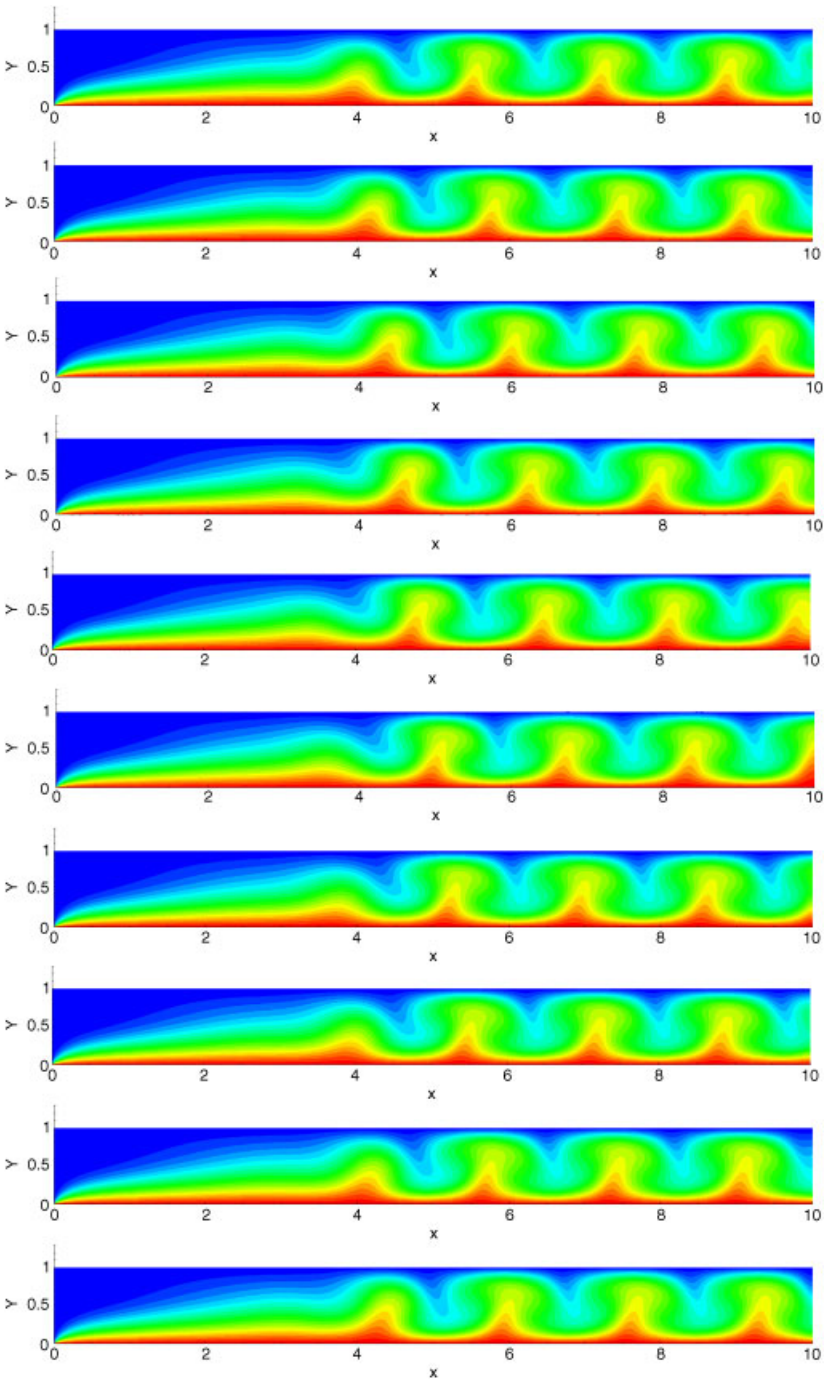


Figure 4. Unsteady experiment with buoyancy: snapshots of isotherms after 12 time units for the experiment with $Re = 5$ and $Gr = 1000$ for the constant-property case.



DOI: 10.1002/fld

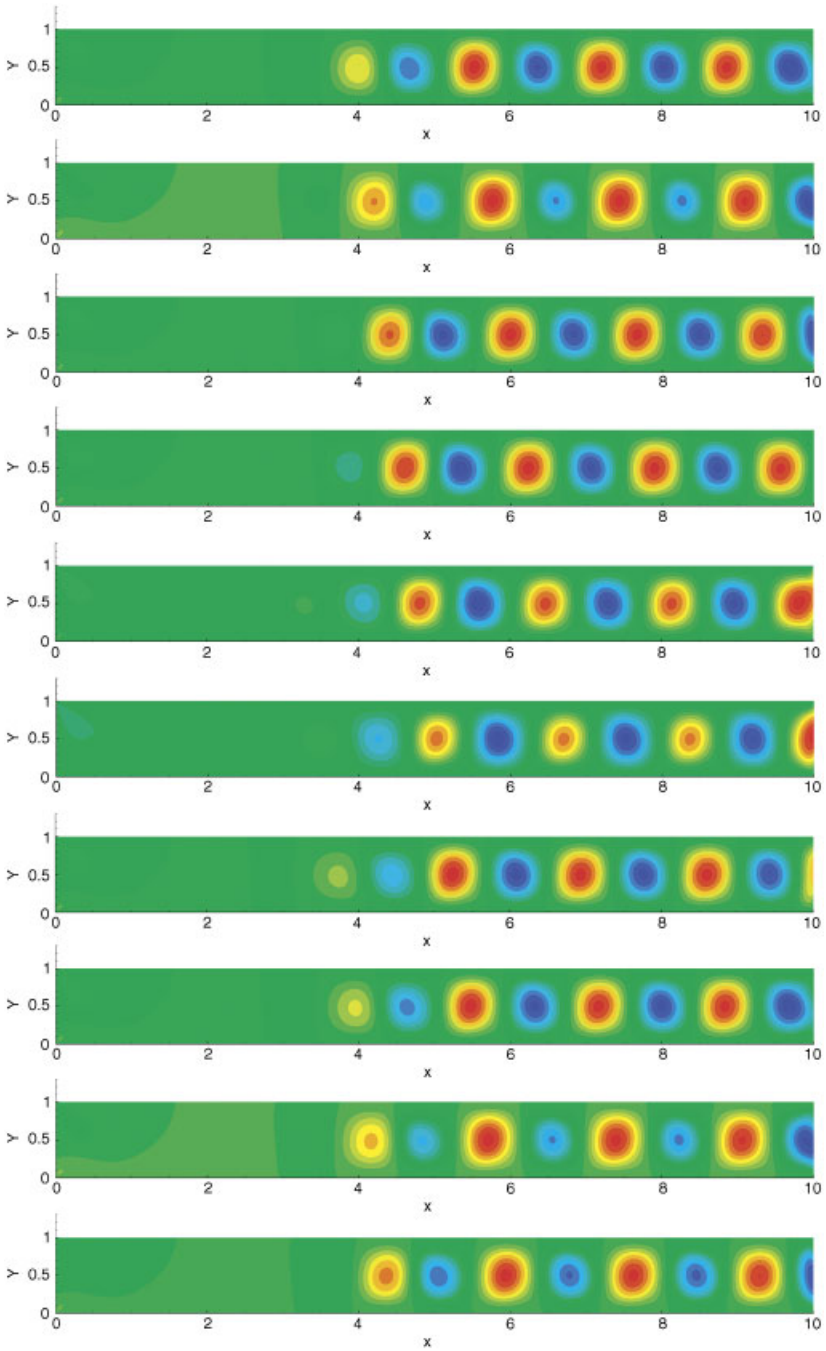


Figure 5. Unsteady experiment with buoyancy: snapshots of the instantaneous radial velocity profiles after 12 time units for the numerical experiment performed with $Re = 5$ and $Gr = 1000$ for the constant-property case.



DOI: 10.1002/fld

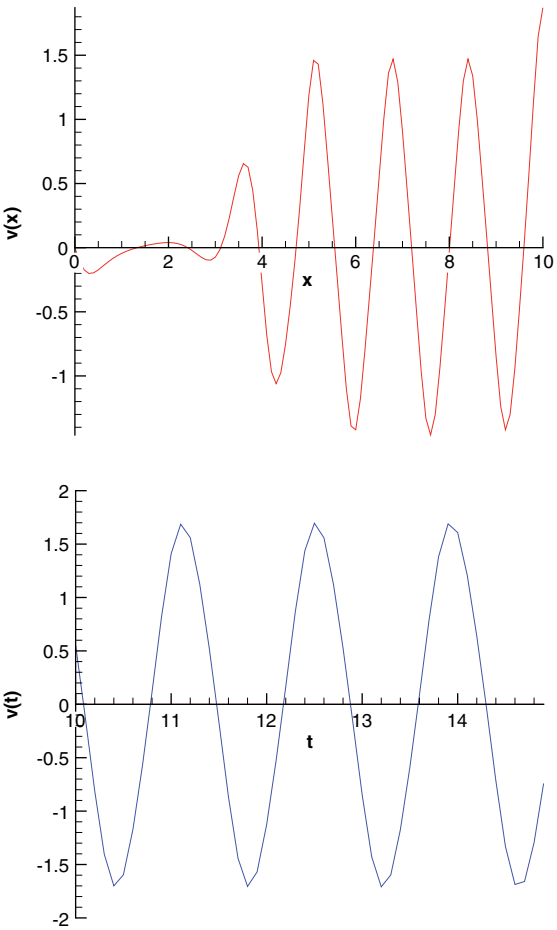


Figure 6. Unsteady experiment with buoyancy: spatial periodicity analysis for the radial velocity and time temporal periodicity analysis at $x = 6$ for the experiment with $Re = 5$ and $Gr = 1000$ for the constant-property case.

without buoyancy. It appears clearly that in this steady analysis the effects are essentially located at the entrance. The maximum velocity moves upwards due to the gravity force whereas the velocity profile is slightly deformed downwards. Moreover, we notice that, compared to the viscosity dependence on temperature ($\mu(T)$), the effect of buoyancy is greater than the opposition by the transverse velocity behaviour $v$.

These figures show clearly the effect of buoyancy. It acts in the direction opposite of $\mu(T)$. Such behaviours are expected and classically obtained in these configurations. But we have to note that if these results are coherent globally, they do not faithfully represent the reality and the great complexity of the flow.

### *4.4. Unsteady results: non-isothermal wall temperature (buoyancy effects)*

For a third numerical experiment, we keep the previous configuration: entry temperature at 20°C, upper wall at 20°C, lower wall at 80°C, and buoyancy effects. The fluid properties are



DOI: 10.1002/fld

considered to be constant. The fluid considered is water, with a Prandtl number taken as 3.57 (water at 50°C).

Figure 4 shows the instantaneous isotherms (10 snapshots) of the flow for a Reynolds number equal to 5 and a Grashof number equal to 1000. These isotherms are obtained after running 12 complete time units, and they can be considered as representatives of the permanent regime. Figure 5 shows the associated instantaneous radial velocity $v(x, y, t)$, which seems to be spatially and temporally periodic.

We can observe in the sequence of snapshots the existence of travelling waves, which are created in the developing zone ($0<x<3$), and correspond to the linear amplification of instabilities, as shown in [40]. This zone is followed by a transitional one ($3<x<4$), and finally, by a saturated zone ($x>4$), where the thermoconvective rolls are established regularly and periodically.

The observed behaviour on these three zones were already noted in [41] when open channel flows were studied.

In Figure 6, the spatial periodicity of the radial velocity $v(x, y, t)$ is shown at different instants. After a fast Fourier transform (FFT) analysis of this radial velocity, we recognize the fundamental frequencies associated with the waves in different sections. Due to this regular spatio-temporal periodicity, we can assume that in the zone where the thermoconvective rolls are established ($x>4$), the radial velocity has the characteristic form of a travelling wave:

$$v(x, y, t) = \tilde{v}(x, y)\mathrm{e}^{\mathrm{i}(kx-\omega t)}$$

Moreover, with the numerical results of this experiment, we can determine the wavelength $\lambda = 1.8$, the wavenumber $k = 3.49$, the temporal period $T = 1.65$ and the pulsation $p = 3.8$. Thus, the corresponding phase velocity is $c = 1.09$. This result is perfectly coherent with those found in the specialized literature (see [42]).

## 5. CONCLUSION

In this second part, we have performed a FE error analysis of the steady coupled problem coming from a generalized Boussinesq model. Some numerical experiments are performed, which show that the effect of the viscosity variations in the fluid are not negligible when buoyancy effects are considered.

For this model, we have stated a general approximation result, which shows that for consistent velocity/pressure FE spaces, the quality of the numerical solution is linked to the approximation properties of the FE subspaces.

Even if the steady buoyancy problem has no physical interest, the results shown in the numerical experiences are in good agreement with well-known dynamic and thermal behaviours (see [39]). The unsteady experiments shown that the unsteady model is consistent with the expected flow dynamics.

Obviously, the richness of this phenomenon lies in the unsteady situation. This aspect will be the subject of future research.

ACKNOWLEDGEMENTS

The authors want to thank the anonymous referees whose comments have helped to improve the quality and the clarity of the paper. This research was partially supported by the Dirección de Investigación of the Universidad de Concepción through the Project DIUC 204.013.022-1.0.



DOI: 10.1002/fld

## REFERENCES


1. Gresho PM, Sani RL. Résumé, remarks on the open boundary condition minisymposium. *International Journal for Numerical Methods in Fluids* 1994; **18**:983–1008.
2. Heywood JG, Rannacher R, Turek S. Artificial boundaries and flux and pressure conditions for the incompressible Navier–Stokes equations. *International Journal for Numerical Methods in Fluids* 1996; **22**:325–352.
3. Bui An Ton B. On the initial boundary-value problem for non-homogeneous incompressible heat-conducting fluids. *Rocky Mountain Journal of Mathematics* 1981; **11**(1):99–112.
4. Diaz JI, Galiano G. On the Boussinesq system with nonlinear thermal diffusion. *Nonlinear Analysis Theory Methods and Applications* 1997; **30**(6):3255–3263.
5. Gaultier M, Lezaun M. Equations de Navier–Stokes couplées à des équations de la chaleur: résolution par une méthode de point fixe en dimension infinie. *Annales des Sciences Mathematicqes du Québec* 1989; **13**(1):1–17.
6. Goncharova ON. Unique solvability of a two-dimensional nonstationary problem for the convection equations with temperature-dependent viscosity. *Differential Equations* 2002; **38**(2):249–258.
7. Lions P-L. *Mathematical Topics in Fluid Dynamics*, *Vol. 1*: *Incompressible Models*. Clarendon Press: Oxford, 1996.
8. Coulliette DL, Koch M. On the difficulties and remedies in enforcing the div=0 condition in the finite element analysis of thermal plumes with strongly temperature-dependent viscosity. *International Journal for Numerical Methods in Fluids* 1994; **18**:189–214.
9. Hossain MA, Munir MS, Hafiz MZ, Takar HS. Flow of a viscous incompressible fluid of temperature dependent viscosity past a permeable wedge with uniform surface heat flux. *Heat and Mass Transfer* 2000; **36**:333–341.
10. Reddy JN, Gartling DK. *The Finite Element Method in Heat Transfer and Fluid Dynamics*. CRC Press: Boca Raton, FL, 1994.
11. White DB. The planforms and onset of convection with a temperature-dependent viscosity. *Journal of Fluid Mechanics* 1988; **191**:247–286.
12. Bruneau C-H. Boundary conditions on artificial frontiers for incompressible and compressible Navier–Stokes equations. *Mathematical Modelling and Numerical Analysis* 2000; **34**(2):303–314.
13. Conca C, Murat F, Pironneau O. The Stokes and Navier–Stokes equations with boundary conditions involving the pressure. *Japanese Journal of Mathematics* 1994; **20**(2):279–318.
14. Gresho PM. On the theory of semi-implicit projection methods for viscous incompressible flow and its implementation via a finite element method that also introduces a nearly consistent mass matrix, Part 1: theory. *International Journal for Numerical Methods in Fluids* 1990; **11**:587–620.
15. Gresho PM. On the theory of semi-implicit projection methods for viscous incompressible flow and its implementation via a finite element method that also introduces a nearly consistent mass matrix, Part 2: implementation. *International Journal for Numerical Methods in Fluids* 1990; **11**:621–659.
16. Pironneau O. *Méthodes des Eléments Finis Pour les Fluides*. Masson: Paris, 1988.
17. Alekseev GV, Smishliaev AB. Solvability of the boundary-value problems for the Boussinesq equations with inhomogeneous boundary conditions. *Journal of Mathematical Fluid Mechanics* 2001; **3**:18–39.
18. Bernardi C, Métivet B, Pernaud-Thomas B. Couplage des équations de Navier–Stokes et de la chaleur: le modèle et son approximation par Eléments Finis. *Mathematical Modelling and Numerical Analysis* 1995; **29**(7):871–921.
19. Blancher S, Creff R, Pérez CE, Thomas J-M. The steady Navier–Stokes/energy system with temperature-dependent viscosity—Part 1: analysis of the continuous problem. *International Journal for Numerical Methods in Fluids* 2007; DOI: 10.1002/fld.1509.
20. Ciarlet PG. *Mathematical Elasticity*, *Volume I*: *Three-dimensional Elasticity*. Studies in Mathematics and its Applications, vol. 20. North Holland: Amsterdam, 1988.
21. Duvaut G, Lions J-L. Transfert de chaleur dans un fluide de Bingham dont la viscosité dépend de la température. *Journal of Functional Analysis* 1972; **11**:93–110.
22. Bruneau C-H, Fabrie P. Effective downstream boundary conditions for incompressible Navier–Stokes equations. *International Journal for Numerical Methods in Fluids* 1994; **19**:693–705.
23. Girault V, Raviart PA. *Finite Element Methods for Navier–Stokes Equations* (2nd edn). Springer: Berlin, 1986.
24. Xu X. A discrete Korn's inequality in two and three dimensions. *Applied Mathematics Letters* 2000; **13**:99–102.
25. Grisvard P. *Elliptic Problems in Nonsmooth Domains*. Monographs and Studies in Mathematics, vol. 24. Pitman: London, 1985.
26. Brezzi F, Fortin M. *Mixed and Hybrid Finite Element Methods*. Springer: Berlin, Heidelberg, New York, 1991.
27. Ern A, Guermond J-L. *Eléments Finis*: *Théorie*, *Applications*, *Mise en Oeuvre*. Mathématiques and Applications, vol. 36. Springer: Berlin, 2002.

28. Thomas J-M. Sur l'analyse numérique des méthodes d'éléments finis hybrides et mixtes. *Ph.D. Thesis*, Thèse de Doctorat d'Etat, Université Paris VI, 1977.
29. Pérez CE. Analyse Numérique de Phénomènes de Couplage liés aux Transferts Thermiques. *Ph.D. Thesis*, Thèse, Université de Pau et des Pays de l'Adour, 2003.
30. Boffi D, Gastaldi L. On the quadrilateral Q2-P1 element for the Stokes problem. *International Journal for Numerical Methods in Fluids* 2002; **39**(11):1001–1011.
31. Fortin M, Fortin A. Experiments with several elements for viscous incompressible flows. *International Journal for Numerical Methods in Fluids* 1985; **5**:911–928.
32. Pelletier D, Fortin A, Camarero R. Are FEM solutions of incompressible flows really incompressible? (or how simple flows can cause headaches). *International Journal for Numerical Methods in Fluids* 1989; **9**:99–112.
33. Gresho PM, Sani RL. *Incompressible Flow and the Finite Element Method*, *Volume Two*: *Isothermal Laminar Flow* (1st edn). Wiley: New York, 1999.
34. Sleijpen G, Fokkema D. BiCGstab($\ell$) for linear equations involving unsymmetric matrices with complex spectrum. *Electronic Transactions on Numerical Analysis* 1993; **1**(Sept.):11–32 (electronic only).
35. Vuik C. Solution of the discretised incompressible Navier–Stokes equations with the GMRES method. *International Journal for Numerical Methods in Fluids* 1993; **16**(6):507–523.
36. Lide DR (ed.). *CRC Handbook of Chemistry and Physics* (82nd edn). CRC Press: Boca Raton, FL, 1998.
37. Reid RC, Prausnitz JM, Sherwood TK. *The Properties of Gases and Liquids* (3rd edn). McGraw-Hill: New York, 1987.
38. Pinarbasi A, Liakopoulos A. The role of variable viscosity in the stability of channel flow. *International Communications in Heat and Mass Transfer* 1995; **22**(6):837–847.
39. Kakac S, Shah RK, Aung W. *Handbook of Single Phase Convective Heat Transfer*. Wiley-Interscience: New York, 1987.
40. Muller HW, Lucke M, Kamps M. The effect of throughflow on Rayleigh–Bénard convective rolls. In *Ordered and Turbulent Patterns in Taylor–Couette Flow*, Hayot F, Andereck CD (eds), NATO ASI Series, vol. B297. Plenum: NY, 1992; 187–196.
41. Deissler RJ. Spatially growing waves, intermittency, and convective chaos in an open-flow system. *Physica* 1987; **25D**:233–260.
42. Nicolas X. Revue bibliographique sur les écoulements de Poiseuille–Rayleigh–Bénard: écoulements de convection mixte en conduites rectangulaires horizontales chauffés par le bas. *International Journal of Thermal Sciences* 2002; **41**:961–1016.



DOI: 10.1002/fld